단결정 압전작동기를 사용한 능동 뒷전플랩 블레이드의 진동하중 감소해석

Vibratory Loads Reduction Analysis of Active Trailing-edge Flap Blades Using Single Crystal Piezoelectric Actuators

박재상† ·김태성*·신상준**

JaeSang Park, TaeSeong Kim, and SangJoon Shin

Key Words : Single crystal piezoelectric materials, L-L actuator, Active trailing-edge flap blade, Vibratory loads reduction

ABSTRACT

This paper conducts a vibratory loads reduction analysis of an Advanced Active Trailing-edge Flap (AATF) blade utilizing single crystal piezoelectric actuators. For an AATF blade, a new L-L piezostack actuator using single crystal PMN-PT materials is designed. The AATF blade is designed to have similar characteristics to the Advanced Active Twist Rotor (AATR) blade. The active trailing-edge flap is assumed to be 20% of the blade span and 15% of the chord, located at 75% of the blade radius. In order to conduct the vibratory loads reduction analysis of the AATF blade in forward flight, DYMORE, a multi-body dynamics analysis code, is used. The simulation result shows that the hub vibratory loads may be reduced by approximately 89% even with a much lower input-voltage when comparing with the other active rotor systems.

1. Introduction

High vibratory loads and acoustic noise of helicopters during forward flight condition are one of the challenging problems for the modern rotorcraft researchers. To alleviate such high vibratory loads on the fixed- and rotating- systems, during the last two decades, an Active Trailing-edge Flap (ATF, Figure 1) blade has been studied extensively [1-3].

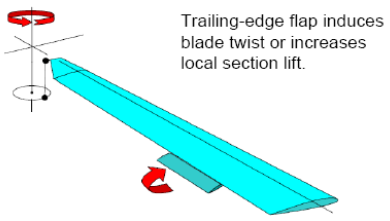

Figure 1 Active Trailing-edge Flap (ATF) blade

This concept uses a small flap on each blade to generate the desirable unsteady aerodynamic loads. By introducing piezoelectric materials which is one sort of the smart materials, the ATF blade is more effective to reduce the vibratory loads as compared with those under the conventional Individual Blade Control (IBC) techniques. In this approach, a partial span trailing-edge flap is located at the outboard region of the blade. The active flap control inputs affect the blade inertial loads and rotor dynamics as well as the unsteady aerodynamic loads.

In order to deflect a rotor blade trailing-edge flap, over the past decade, various piezoelectric actuators have been developed. Piezoelectric bender actuators (Figure 2) were developed for the small scale wind tunnel models [4-6]. Piezoelectric benders consists of two or more piezoelectric sheets stacked together such that actuating the layers on opposite sides of the neutral axis results in an opposite strain which may cause the entire bender to be deflected. After improvements in the actuator design, approximately ±4° flap deflections were obtained at a rotor speed of 1800 RPM [5]. Closed loop wind tunnel tests showed a dramatic vibration reduction in 4/rev fixed frame loads.

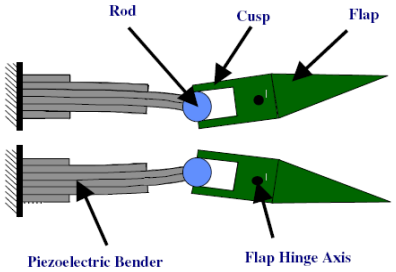

Figure 2 Schematic diagram of a trailing-edge flap using the piezoelectric bender

As another type of piezoelectric actuator, there are piezoelectric stack actuators constructed by laminating multiple piezoelectric layers (Figure 3). The piezostack actuators can be used in the small- or full-scaled models and have a larger force output than the bender actuators. However, they can only produce a relatively small

† 서울대학교 기계항공공학부, 박사후 연구원
E-mail : tux2000@snu.ac.kr
Tel : (02) 880-1901, Fax : (02) 887-2662

* 서울대학교 기계항공공학부, 박사과정 대학원생

** 서울대학교 기계항공공학부, 조교수

displacement, and that should be amplified in order to achieve a required flap deflection. This limitation needs more complex amplification mechanisms than the benders.

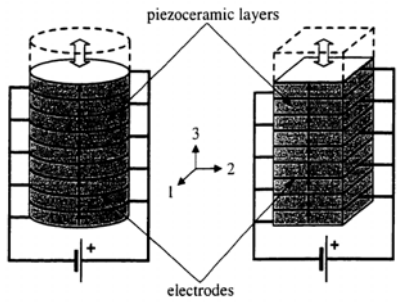

Figure 3 Schematic of the piezoelectric stacks

By using piezostack actuator, Lee and Chopra developed the uni-directional double-lever actuator (L-L actuator, [7], Figure 4) and bi-directional double-lever actuator [8]. The actuator utilizes a set of linkages that converts the radial displacement of the stack to the flap deflection and has a theoretical amplification ratio of 30. The L-L actuator was applied in Boeing MD Explorer and produces approximately ±6° flap deflection during the bench test.

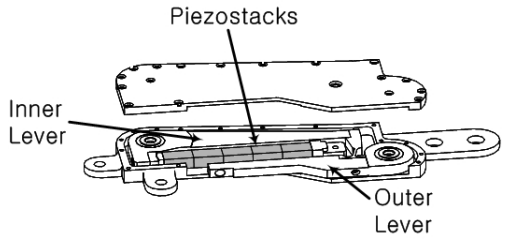

Figure 4 Schematic of a uni-directional L-L actuator

The new piezoelectric materials, single crystal piezoelectric materials [9], have been developed recently. Those are capable of producing strain levels more than 1% and which exhibit five times larger than that of the conventional piezoceramic materials in terms of strain energy density. In addition, they have higher coupling constants. Although it is still difficult to manufacture the single crystal piezoelectric materials in large quantities and complex geometries, it will be advantageous to use such improved actuation performance of the piezostack flap actuator.

Therefore, in this paper, a new L-L actuator utilizing a single crystal PMN-PT stack is designed in a relatively simple way and the vibratory loads reduction analysis of an Advanced Active Trailing-edge Flap (AATF) blade using the new L-L actuator is conducted. In the AATF blade, it is assumed that the blade characteristics are similar to those of the Advanced Active Twist Rotor (AATR, [10]) blade. The active trailing-edge flap is assumed to be 20% of the blade span and 15% of the chord, located at 75% of the blade radius. In order to conduct the aeroelastic analysis of the AATF blade in forward flight, DYMORE, a multi-body dynamics code [11], is utilized. Flap modeling requires an introduction of several rigid joints and elastic beams which will be discussed in detail later. Through the vibratory loads reduction analysis, the most effective flap actuation frequency and phase angle are investigated to obtain the minimum hub vibratory loads.

2. Modeling of the actuator and AATF blade

2.1 Design of a new L-L actuator

A new L-L actuator using single crystal PMN-PT stacks is designed to be applied to the present AATF blade (Radius = 1.397 m, Chord = 0.1175 m). Figure 5 shows the schematic representation of the L-L amplification mechanism [7]. Since the new L-L actuator should be located inside the active trailing-edge flap, its length with respect to the radial direction should not exceed the flap length. Therefore, due to this limitation, $L_a = 0.0423$, $L_b = L_d = 0.2115$, $L_c = 0.0352\,[m]$ are selected in this design.

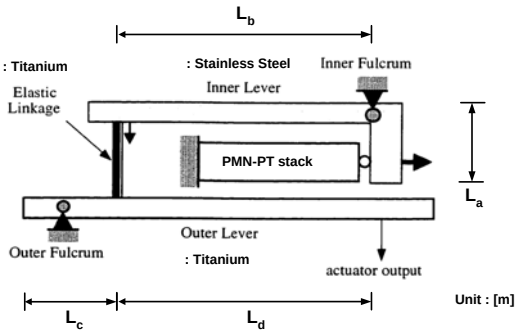

Figure 5 L-L amplification mechanism

The kinematic gains of Inner Lever and Outer Lever are defined in Eq. (1). Above design values give a theoretical amplification ratio of 30.

$$G_1 = \frac{L_b}{L_a} \tag{1a}$$

$$G_2 = \frac{L_d}{L_c} \tag{1b}$$

The output displacement u_e can be expressed as

$$u_e = \frac{u_0 G_1 G_2}{1 + \frac{k_e}{k_d} + G_2^{\,2}\left(\frac{k_e}{k_m} + \frac{k_e}{k_b} + \frac{k_e}{k_c}\right) + \left(G_1 G_2\right)^2 \left(\frac{k_e}{k_p} + \frac{k_e}{k_a}\right)} \tag{2}$$

where u_0 and k_p are the free actuation displacement and the stiffness of the PMN-PT stack, respectively.

Finally, the trailing-edge flap deflection can be determined as shown in Eq. (3) and Figure 6.

$$\delta = \frac{u_e}{e} \tag{3}$$

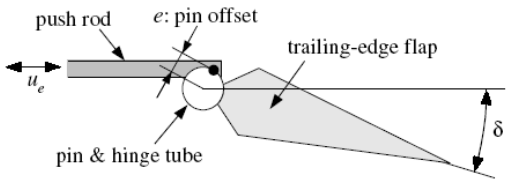

Figure 6 Relationship between the flap deflection and resulting displacement

2.2 DYMORE modeling for AATF blade

In this work, through direct time integration, DYMORE analyzes the forward flight response of the AATF blade. Figure 7 shows the DYMORE model for the four-bladed AATF system for forward flight time domain analysis and detailed trailing-edge flap representation.

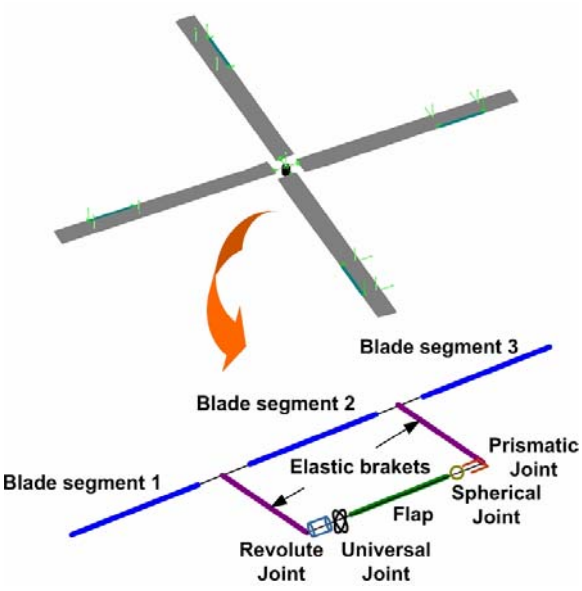

Figure 7 AATF modeling in DYMORE

The hub is modeled as a rigid body, and connected with a revolute joint underneath. It is under a prescribed rotation with nominal rotating speed Ω. Root retention is a passive elastic beam rigidly attached to the hub, and the reaction loads at the attachment point are extracted and added over four of them to give the hub vibratory loads. Because the AATF rotor system is fully articulated, three revolute joints are consecutively located between the root retention and the active flap blade to represent flap, lead-lag, and feathering hinges.

In this modeling, the flapping and lead-lag hinges are coincident. Active blades are attached to represent the AATF blades, and they can be divided into 3 regions: passive inner blade (blade segment 1), active flap blade (blade segment 2) and passive outer blade (blade segment 3) regions. Each blade region is discretized during the analysis at least three beam elements per blade, each with the 3rd-order interpolation polynomials. Finally, to represent trailing-edge flap in DYMORE, as shown in Figure 7, several rigid joints and elastic beams for the brackets and flap are introduced. The flap is assumed to be 20% of the blade span and 15% of the chord, located at 75% of the blade radius.

In DYMORE, the formulation of beams is geometrically exact (arbitrarily large displacements and finite rotations are considered), but is limited to small strains. For the aerodynamic modeling, Peters and He's the finite-state dynamic inflow aerodynamic model is used. The equation motions are formulated in a Cartesian inertial frame. Constraints are implemented using the Lagrange multiplier technique.

The AATF blade is assumed that the blade characteristics are similar to those of the AATR blade [10] utilizing single crystal Macro Fiber Composites (MFC). Table 1 describes the general properties of the AATR blade.

Table 1 Properties of the AATR blade

Rotor type	Fully articulated
Number of blades, b	4
Blade chord, c	0.1175 m
Blade radius, R	1.397 m
Solidity, bc/πR	0.0982
Lock number	9.0
Airfoil shape	RC Airfoil
Blade linear pretwist	-10 deg.
Hinge offset	7.62 cm
Root cutout	31.75 cm
Pitch axis	25.0% c
Elastic axis	27.9% c
Center of gravity	28.0% c
Nominal rotor speed	687.5 RPM
1st torsional frequency at nominal rotor speed	4.87/rev
Maximum strain	4995 μstrain

In addition, to efficiently impose an IBC-mode sine-dwell signal with control phase variation, a series of

input-voltage is generated using the following formula:

$$V(t) = V_{\text{amplitude}} \times \cos\left\{2\pi\omega_{\text{actuation}}(t - \phi_{\text{control phase}}) + 2N_{\text{act}}\pi\phi_{\text{blade}\,i}\right\} \quad (4)$$

An example of the input-voltage signal generated for an IBC-mode 3P (=3/rev) actuation with 12 divisions of control phase is shown in Figure 8. No actuation is applied for the initial 3 seconds to establish a steady-state equilibrium for the given flight condition. For each 0.5-s period of actuation, each with different control phase angle, and another 0.5-s period of no actuation is applied between them.

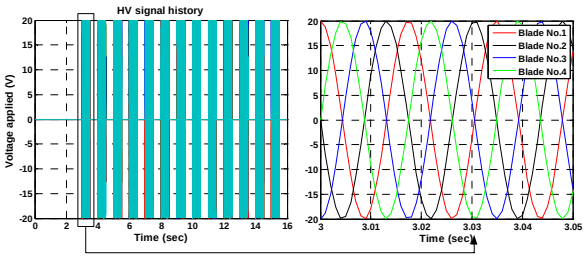

Figure 8 Example of an input-voltage generated for an IBC 3P actuation with 12 divisions of control phase angle

3. Numerical Results

3.1 Actuation performance of the new L-L actuator

In this section, actuation performance of the new L-L actuator utilizing single crystal PMN-PT stack is compared with the result of the L-L actuator with PZT-5A stack. Table 2 gives material properties of PMN-PT and PZT-5A for piezostacks of L-L actuators.

Table 2 Material properties of PMN-PT and PZT-5A [12]

Property	PMN-PT	PZT-5A
E [GPa]	8.33	53
G [GPa]	3.18	21
ν	0.310	0.384
ρ [kg/m^3]	8200	7800
d_{33} [pm/V]	2000	390
d_{31} [pm/V]	-950	-190

Figure 9 shows the relationship between input-voltage and flap deflection angle. In this paper, the target flap deflection angle is selected as ±4°. As one can see, in order to achieve the target flap deflection angle, the designed L-L actuator using single crystal PMN-PT stack requires the amplitude of input-voltage of only 20 V, however the L-L actuator using PZT-5A stack will achieve the target deflection angle with the amplitude of input-voltage 100V. Therefore, for the target flap deflection, the new L-L actuator using single crystal PMN-PT stack only requires an input-voltage 20% relative to that for the L-L actuator with PZT-5A stack.

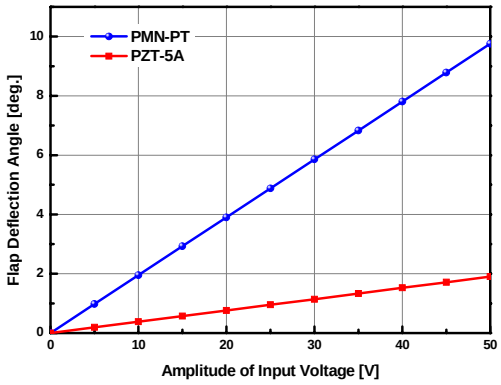

Figure 9 Flap deflection angle in terms of the amplitude of an input-voltage

3.2 Vibratory loads reduction analysis

Since the simple design of the new L-L actuator utilizing single crystal PMN-PT stack is completed, in this section, vibratory loads reduction of the AATF blade in forward flight is investigated. Specifically, hub reaction loads of the rotor system are estimated. These vibratory loads are obtained from summation of all the loads in the four root retention elements. Figure 10 illustrates the simulated vertical component of the hub shear forces developed in the AATF system when 3P sine-dwell actuation is applied as shown in Figure 8.

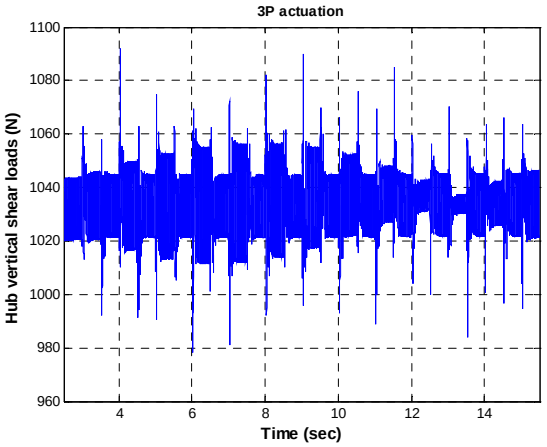

Figure 10 Simulated time history of the hub vertical shear loads with 3P actuation

For this example, the amplitude of input-voltage is 20 V. In addition, the steady-state trim condition is advance ratio $\mu = 0.140$, rotor-shaft angle of attack $\alpha_s = -1°$ and thrust coefficient $C_T = 0.0066$.

This time domain analysis result can be transferred to frequency domain to investigate the magnitude of the frequency content of interest, which is 4P in the present four-bladed rotor system. Figure 11 shows 4P hub shear vibratory loads with 3P, 4P and 5P actuation during the same steady-state trim condition. Here, 'baseline' represents the values extracted during the last period of this interval, say between 2.5 and 3.0s.

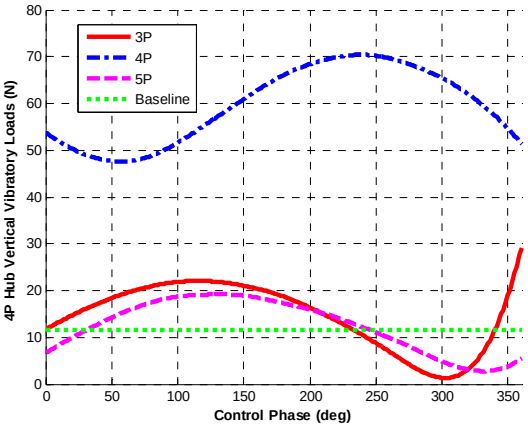

(a) Vertical

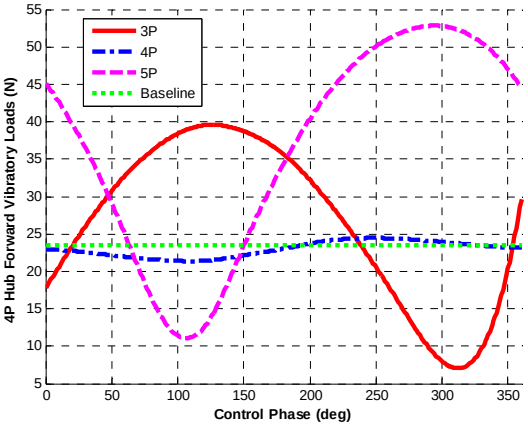

(b) Forward

Figure 11 Variation of 4P hub shear vibratory loads with 40 V_{pp} actuation at 3P, 4P and 5P with respect to control phase

As one can see, 3P actuation appears to be the most effective in reducing the hub shear vibratory loads in both cases of vertical and forward components. Particularly, as compared with the baseline value, 3P actuation with 303° control phase gives approximately 89% reduction of the hub vertical shear load. Furthermore, 3P actuation with 313° control phase reduces the hub forward shear load by 70%.

It should be noticed that these vibratory loads reduction can be obtained when only 40 V_{pp} input-voltage is imposed on AATF system. To achieve this level of the vibratory loads reduction, if the ATF blade using conventional PZT stacks is considered, 200~300V_{pp} input-voltage is required in general. Furthermore, as compared with the ATR controls, the original ATR blade [13] using Active Fiber Composites (AFC) and the AATR blade require 2,000 and 200V_{pp} twist actuations, respectively. Since the single crystal PMN-PT material has excellent actuation performance, the AATF blade is capable of reducing the vibratory loads of rotorcrafts more efficiently.

4. Conclusion

In this paper, the vibratory loads reduction analysis of the AATF blade utilizing single crystal PMN-PT piezostack actuator is conducted. For the trailing-edge flap of the AATF blade, the new L-L actuator using single crystal PMN-PT stack is designed in a relatively simple way. By comparing the conventional L-L actuator with PZT-5A stack, the new L-L actuator can achieve the target flap deflection, ±4°, only with 20% smaller input-voltage of the L-L actuator compared with that for PZT-5A stack. Through an aeroelastic analysis of the AATF blade using the designed L-L actuator, the vibratory loads reduction capability and efficiency in forward flight condition are investigated. As a result, the AATF blade reduces the 4/rev hub vertical vibratory loads by 89% when 3/rev actuation frequency and 303 deg. phase angle are applied to the active flap. When comparing with the other active rotor systems, the simulation result indicates that the AATF blade requires quite lower input-voltage to obtain the sufficient vibratory loads reduction in rotorcraft.

Acknowledgement

This work was supported by Brain Korea 21 Project in 2007, KARI under KHP Dual-Use Component Development Program funded by the MOCIE, and the Korea Science and Engineering Foundation (KOSEF) grant funded by the Korea Government (MOST) (F01-2007-000-10077-0).

References

[1] Chopra, I., "Status of Application of Smart Structures Technology to Rotorcraft Systems," Journal of the American Helicopter Society, Vol.

45, 2000, pp. 228-252
[2] Straub, F. K., Kennedy, D. K., Stemple, A. D., Anand, V. R., Birchette, T. S., "Development and whirl tower test of the SMART active flap rotor," SPIE Annual International Symposium on Smart Structures and Materials, San Diego, CA, 2004.
[3] Dieterich, O., Enenkl, B., Roth, D., "Trailing Edge Flaps for Active Rotor Control Aeroelastic Characteristics of the ADASYS Rotor System," American Helicopter Society 62nd Annual Forum, Phoenix, AZ, May 2006.
[4] Samak, D. K., Chopra, I., "Design of High Force, High Displacement Actuators for Helicopter Rotors," Smart Structures and Intelligent Systems; Proceedings of the Conference, Orlando, FL, Feb, 1994.
[5] Koratkar, N. A., Chopra, I., "Wind Tunnel Testing of a Smart Rotor Model with Trailing-Edge Flpas," Journal of the American Helicopter Society, Vol. 47, (4), 2002, pp. 263-272.
[6] Hall, S. R., Spangler, R., "Piezoelectric Actuators for Helicopter Rotor Control," 31st AIAA/ASME/ASCE/AHS/ASC Structures, Structural Dynamics and Materials Conference, Long Beach, CA, April 1990.
[7] Lee, T.-O., Chopra, I., "Design Issues of a High-Stroke, On-Blade Piezostack Actuator for a Helicopter Rotor with Trailing-Edge Flaps," Journal of Intelligent Material Systems and Structures, Vol. 11, 2000, pp. 328-342.
[8] Lee, T.-O., Chopra, I., "Designs of a Bidirectional Piezoelectric Actuator for Blade Trailing-Edge Flap," SPIE Annual International Symposium on Smart Structures and Materials, San Diego, CA, 2001.
[9] Li, T., Scotch, A. M., Chan, H. M., Harmer, M. P., Park, S.-E., Shrout, T. R., and Michael, S. J., "Single Crystals of $Pb(Mg_{1/3}Nb_{2/3})O_3$-35 mol% $PbTiO_3$ from Polycrystalline Precursors," Journal of American Ceramic Society, Vol. 81, 1998, pp. 244-248.
[10] Park, J.-S., and Shin, S.-J., "Preliminary Design Optimization on Active Twist Rotor Blades Incorporating Single Crystal Macro Fiber Composites," American Helicopter Society 63rd Virginia Beach, VA, May, 2007.
[11] Bauchau, O. A., "DYMORE Manual," http://www.ae.gatech.edu/people/obauchau/ Dwnld/ DymoreManual.pdf, 2007.
[12] TRS Ceramics, Inc. http://www.trsceramics.com
[13] Wilbur, M. L., Mirick, P. H., Yeager, Jr. W. T., Langston, C. W., Cesnik, C. E. S., and Shin, S.-J., "Vibratory Loads Reduction Testing of the NASA/Army/MIT Active Twist Rotor," Journal of the American Helicopter Society, Vol. 47, (2), 2002, pp. 123-133.